Quaestiones Geographiceae

SPATIAL PATTERNS OF URBAN THERMAL COMFORT OVER TROPICAL CITY, CASE STUDY IN HO CHI MINH CITY, VIETNAM

--Manuscript Draft--

Manuscript Number:	QG-D-22-00021
Full Title:	SPATIAL PATTERNS OF URBAN THERMAL COMFORT OVER TROPICAL CITY, CASE STUDY IN HO CHI MINH CITY, VIETNAM
Article Type:	Original Study
Section/Category:	Physical Geography and Geoinformation (GIS)
Keywords:	Correlation analysis; discomfort index; meteorological parameters; remote sensing; urban landscape; urban thermal environment
Abstract:	Urbanization and human activities in urban environments along with climate change are increasing thermal discomfort, negatively affecting work performance, safety, and human health. The paper presents the use of Landsat satellite data to evaluate the spatial patterns of urban thermal comfort (UTC) by estimating Thom's discomfort index (DI) for the North of Ho Chi Minh City (NHCMC). In this study, we focused on outdoor thermal comfort over a large spatial area of the city. The index was established based on meteorological parameters of air temperature and relative humidity determined from satellite images through the correlation between surface temperature, vegetation index, and in-situ data from meteorological stations. The results found that UTC spatial patterns were distributed differently in each NHCMC zone and showed a relationship between the land cover and thermal comfort distribution. The thermal Discomfort of the urban environment has been pronounced chiefly in the urban districts with high building density and focused industrial zones. Conversely, the suburban area usually possessed high vegetation and water covers, presenting a higher thermal comfort level. These results can provide a scientific basis for optimizing urban landscape management in a tropical city like Ho Chi Minh City in the context of increasingly severe climate change to serve a better quality of life.

SPATIAL PATTERNS OF URBAN THERMAL COMFORT OVER TROPICAL CITY, CASE STUDY IN HO CHI MINH CITY, VIETNAM

ABSTRACT: Urbanization and human activities in urban environments along with climate change are increasing thermal discomfort, negatively affecting work performance, safety, and human health. The paper presents the use of Landsat satellite data to evaluate the spatial patterns of urban thermal comfort (UTC) by estimating Thom's discomfort index (DI) for the North of Ho Chi Minh City (NHCMC). In this study, we focused on outdoor thermal comfort over a large spatial area of the city. The index was established based on meteorological parameters of air temperature and relative humidity determined from satellite images through the correlation between surface temperature, vegetation index, and in-situ data from meteorological stations. The results found that UTC spatial patterns were distributed differently in each NHCMC zone and showed a relationship between the land cover and thermal comfort distribution. The thermal Discomfort of the urban environment has been pronounced chiefly in the urban districts with high building density and focused industrial zones. Conversely, the suburban area usually possessed high vegetation and water covers, presenting a higher thermal comfort level. These results can provide a scientific basis for optimizing urban landscape management in a tropical city like Ho Chi Minh City in the context of increasingly severe climate change to serve a better quality of life.

KEY WORDS: *Correlation analysis, discomfort index, meteorological parameters, remote sensing, urban landscape, urban thermal environment.*

Introduction

Urbanization increases the impervious surfaces that absorb solar radiation, causing the surface to become warmer, along with human activities, making the microclimate inside the city more and more stuffy (Van, 2010). Human activities in hot climates easily lead to stress and reduced work efficiency. The higher the heat stress, the higher the hazards and risks to human health (Pradhan et al., 2013). The human body is essentially a constant temperature device (Bradshaw, 2006). The metabolism continuously produces heat and automatically regulates the dissolution to keep body temperature in a constant range. When people are constantly exposed to a discomfortable thermal environment, they will feel uncomfortable, reduce their work productivity, and danger their lives. Health conditions, occupational safety, and working environment are not only required at the workplace of employees but are more broadly understood as a large open space of an industrial park, a residential area, or a territory. Good quality of life in an open space will give people a sense of security and health in a clean environment (Lee et al., 2015; Nasution and Zahran, 2018). Living and working in a place with low environmental pressure create comfortable and pleasant psychology, increase morale, and work with high productivity. On the contrary, in places where the environmental pressure is too high, people find it difficult to concentrate, get tired, thereby reducing labor productivity. In addition, it can cause other diseases. A disorder of thermoregulation causes heat stroke if the temperature rises to 40-41^{o}C, causing a coma. If not treated promptly, it causes death (National Assembly, 2013). The increasing urban ambient temperature increases the discomfort of the human body. Sick people who do not do manual labor, such as those with heart disease, respiratory disease, chronic disease, malnutrition, diabetes, or the elderly, children and pregnant women, often have less heat tolerance than other people, so they often feel uncomfortable and stuffy when the temperature rises. Therefore, besides noise and air pollution, thermal comfort is considered as one of the important aspects of sustainable

development in urban areas (Mayer et al., 2008). Especially, as the urban is expanding, it is necessary to have an indicator to describe the urban thermal environment.

Many bioclimatic indices can represent thermal comfort, and it is used to quantify the integral effects of heat exchange between the human body and the thermal environment. It is affected by several parameters, including air temperature, wind speed, radiation, humidity, clothing, and activities (Natos, 2006). Many different experimental model studies have evaluated thermal comfort and bioclimatic conditions. Some methods emphasize meteorological parameters, while some complex methods require the appearance of many variations under defined conditions. Some prominent methods are Fanger's "comfort equation" for calculating the predictive mean vote (PMV) (Fanger, 1970); the physiological equivalent temperature (PET), calculated from the Munich energy-balance model for individuals (MEMI) (Hoppe, 1999); the Menex bioclimate index based on the human heat balance (Pecelj, 2013). The Discomfort Index (DI) (Thom, 1959), ThermoHydrometric Index (THI) of Kyle (1994) require temperature and relative humidity data to assess thermal comfort. In addition, there are several other related studies on the dynamical system of heatwaves and UHI (Li and Bou-Zeid, 2013; Keeler, 2012).

Of all the above indicators, Thom's DI is one of the most famous and is an important indicator that measures the human heat sensation for different climate conditions. DI is the most accessible and best index for effective temperature estimation, which is highly objective because it does not depend on subjective human feelings (Stathopoulou et al., 2005; Adegoke and Dombo, 2019). On the other hand, the DI uses two data sources, temperature and relative humidity, widely available in microclimate studies, so it is easy to perform. DI is usually calculated using data from a single or a few weather stations, and it cannot represent the thermal state of the whole city. This limits the DI application (Xu et al., 2017). Remote sensing technology acquiring spatial information and image processing techniques help people detect objects in each specific location to support accurate and timely decisions. These are potential technologies to support suitable DI applications.

In 2004 Wang et al. had an analytical study on the spatial variation of urban human thermal comfort in Hangzhou, China using remote sensing images and the thermal discomfort index DI. The research results have calculated the heat stress index and established Hangzhou city's thermal comfort space map (Wang et al., 2004). Ahmed et al. (2010) studied and compared heat stress conditions in Akure, Nigeria's city center, and rural airport environment. The results indicated the urban heat island effect on Akure as the city center was warmer than the rural airport throughout the day. The frequent occurrence of high temperatures in the city center poses significant environmental heat stress and human health risk in Akure. Similar studies have been published, such as Ifeoluwa et al. (2013), José et al. (2013), Hamidreza et al. (2014). These studies have shown that remote sensing methods are objective, low-cost, and cover a large area.

Therefore, it is necessary to detect and monitor the status of thermal comfort according to spatial models in cities to support the master planning of urban landscapes serving better quality of life. Based on the above analysis, this study explores the use of Landsat satellite data to evaluate the spatial patterns of UTC in different locations of the city by Thom's DI. Besides, the study also considers the distribution of land cover and explores the spatial distribution of UTC on different types of land cover to assist in

developing appropriate solutions to improve the thermal conditions of the urban environment for the study area.

Study area

Ho Chi Minh City (HCMC) is located at coordinates 10°10’ – 10°38’ North and 106°22’ - 106°54’ East, is the southernmost city of Vietnam. HCMC is in the sub-equatorial monsoon tropical region with high temperatures throughout the year and two distinct rainy and dry seasons, which have a profound impact on the landscape environment. Due to the rapid development in the past few decades, many high-rise buildings and roads have been built. In addition, there is an increase in personal vehicles and air conditioners, which trap high temperatures and make the inner city hotter than the surrounding agricultural areas. In recent years, the average temperature of HCMC has increased; there are places where severe heat has appeared with the temperature at 37-38^{o}C. The sultriest weather is at noon when the temperature rises above 36^{o}C. The naturally hot and humid climate coupled with urban heat islands can create extreme temperature conditions, negatively affecting residents and workers. Especially the elderly and young children. As in many parts of the world, climate change is expected to increase the number of hot days and nights in HCMC, prolong the hot season and increase the number of heat waves in the city. All these changes will have dramatic effects on people, livestock, health, water supply, agriculture, and many other systems.

All over HCMC, urban areas are concentrated in the central and northern areas, where human activities take place, making the difference in the thermal environment between rural and urban areas. Therefore, the study focused on this area and named it north of Ho Chi Minh City (NHCMC), including 19 districts and 4 districts, excluding Can Gio district, a mangrove forest on the wetlands of the southern coast. To understand the spatial distribution of thermal comfort levels, the study will also look at urban subdivisions, specifically: Z1: 13 existing urban districts; Z2: 6 newly developed urban districts; Z3: 4 suburban districts (*Fig. 1*). The names of the zones are named according to Decision 24/QD-TTg in 2010 approving the adjustment of the construction master plan of HCMC until 2025 (Prime Minister, 2010).

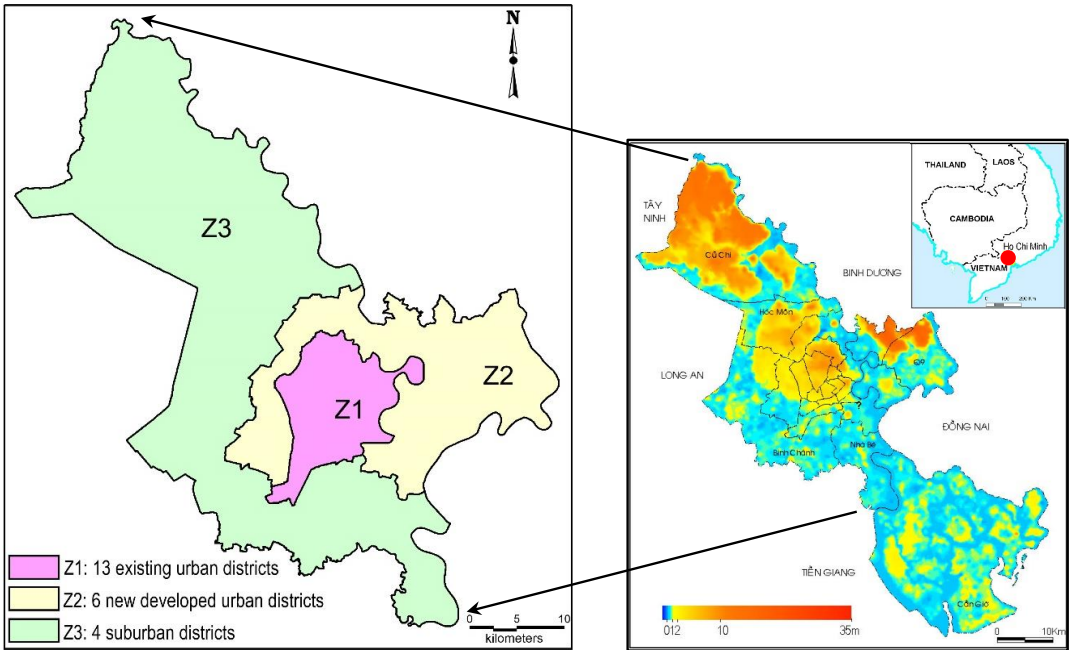

(a)

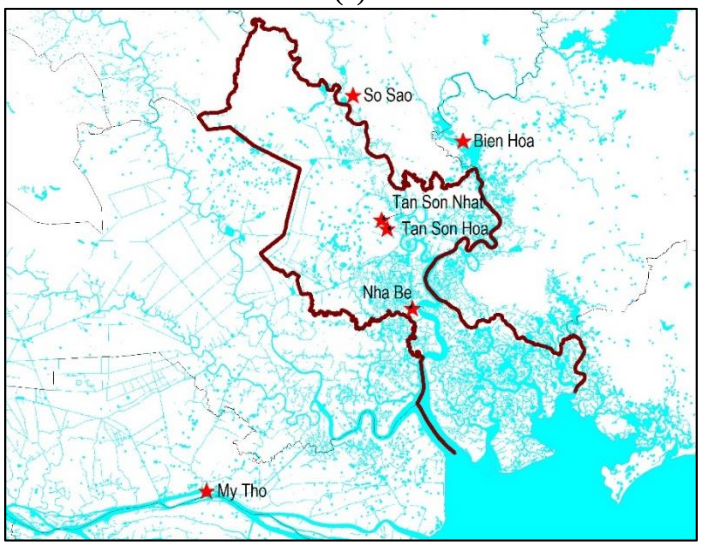

(b)

Fig. 1. (a) The geographical extent of the study area centered on the north of Ho Chi Minh City. The extend of the study area was shown in the topography map of the whole city, which was the red point in the small map in the upper right, belonging south of Vietnam. (b) The lower map points to the location of meteorological stations related to the collected data

Data

For this study, the primary data source used was the satellite imagery of the Landsat program. Landsat is a mission for a system of satellites dedicated to exploring Earth resources and the environment managed by NASA in collaboration with the US Geological Survey since 1972 (Campbell, 1987). Landsat optical imagery is easily affected by atmospheric conditions, so it is necessary to choose the right time to get good quality, cloud-free images right in the study area. HCMC is located in an area with

a tropical monsoon climate typical for Southern weather, with two distinct rainy and dry seasons. The rainy season starts from May to November, and the dry season starts from December to April next year. The rainy season weather is often covered by clouds in the sky, making it difficult to choose good images. Therefore, this study selected images in the dry season. Besides, in this season, the weather is often hot, so the manifestations of heat stress are more likely to occur, so it is suitable for the consideration of thermal comfort.

The main research period is 2019, and the image acquired on January 19, 2019, was obtained from the United States Geological Survey (USGS) Earth observation website (http://earthexplorer.usgs.gov). The image used is the Operational Land Imager and Thermal Infrared Sensor (OLI&TIRS) of the Landsat 8 satellite. The OLI collects image data for eight shortwave bands with a 30m spatial resolution and one with a 15m panchromatic band. The TIRS collects image data for two longwave thermal bands with a 100m resolution (USGS 2021). In addition, the Landsat Thematic Mapper/Enhanced Thematic Mapper (TM/ETM+) images from 1989-2015 were also used to extract data to perform correlation and construct parametric images used in the calculations as air temperature and air humidity. NHCMC is positioned on two scenes of path/row as 125/052 and 125/053 (Table 1)

Alongside Landsat images acquired at 10 am, air temperature and relative humidity measurements were obtained from 6 national meteorological stations within and around the city collected by the Southern Regional Hydrometeorological Center. They are used to build a regression function with parameters extracted from satellite images, as shown in Table 1, and evaluate the accuracy of estimated air temperature and relative humidity images. The image acquisition time over HCMC is around 10 am, so observations from meteorological stations were also selected simultaneously. Locations of meteorological stations are shown in Fig. 1 and Table 2.

Table 1. Collected Landsat image characteristics used in extracting value for calculating Ta and Rh

Acquisition time	Path/Row	Landsat spacecraft	Pixel size of the visible-infrared and thermal band (m)
16/01/1989	125/052	TM 5	30, 120
16/01/1989	125/053	TM 5	30, 120
02/02/1995	125/052	TM 5	30, 120
02/02/1995	125/053	TM 5	30, 120
25/01/1998	125/052	TM 5	30, 120
25/01/1998	125/053	TM 5	30, 120
13/02/2002	125/052	ETM+ 7	30, 60
13/02/2002	125/053	ETM+ 7	30, 60
04/01/2005	125/052	ETM+ 7	30, 60
04/01/2005	125/053	ETM+ 7	30, 60
25/12/2006	125/052	ETM+ 7	30, 60
25/12/2006	125/053	ETM+ 7	30, 60
24/1/2015	125/052	L8 OLI&TIRS	30, 100
24/1/2015	125/053	L8 OLI&TIRS	30, 100
29/03/2015	125/052	L8 OLI&TIRS	30, 100
29/03/2015	125/053	L8 OLI&TIRS	30, 100

Table 2. National meteorological stations used in the study

Station	Longitude	Latitude	Land cover type around the station	Used in the study
Tan Son Nhat	106º39'39"	10º49'11"	Built-up	Regression analysis and accuracy evaluation
Tan Son Hoa	106º42'00"	10º49'00"	Built-up	Regression analysis and accuracy evaluation
So Sao	106º39'01'	10º59'39"	Vegetation (rural)	Regression analysis
Bien Hoa	106º49'30"	10º57'25"	Built-up	Regression analysis
My Tho	106º23'00"	10º21'00"	Vegetation (rural)	Regression analysis
Nha Be	106º43'39"	10º39'32"	Vegetation (rural)	Accuracy evaluation

Methods

Discomfort index

Thom's discomfort index (DI) is expressed by a simple linear equation based on dry-bulb (T_{dry}) and wet-bulb (T_{wet}) temperatures. Its original form was as Equation 1 (Thom, 1959):

$$DI = 0.4 * (T_{dry} + T_{wet}) + 15 \quad \text{(Eq.1)}$$

If air temperature (Ta) measured in degrees Celsius and relative humidity (Rh) in % are given, DI can be computed by using equation 2 (Kyle, 1994; Unger, 1999; Toy et al., 2007). This index estimates the effective temperature and describes the degree of discomfort at various combinations of temperature and humidity.

$$DI = Ta - 0.55 * (1 - 0.01 * Rh) * (Ta - 14.5) \quad \text{(Eq.2)}$$

Thom's discomfort index was the first index created to assess levels of human discomfort related to meteorological variables. It was classified into 6 levels of discomfort conditions from no thermal discomfort to state of medical emergency, as shown in Table 3.

Table 3. Thom's discomfort index classification (Thom 1959)

N	DI classification	DI (ºC)
1	No Discomfort	< 21
2	Under 50% of Population feels discomfort	21 - 24
3	Over 50% of Population feels discomfort	24 - 27
4	Most of the Population feels discomfort	27 - 29
5	Everyone feels stress	29 - 32
6	State of medical emergency	>32

However, each country has certain natural and climatic conditions, so applying this thermal comfort classification to HCMC is inappropriate. In this study, we investigated the climatic conditions in HCMC, then built thermal comfort levels based on the scale of new effective temperature corresponding to physiological response and body health according to the document on bioclimatic architectural design applied to Vietnam by Nguyen (2008). Accordingly, the new effective temperature of a space is defined as the dry temperature of an equivalent thermal environment at 50% humidity, and with

uniform radiation conditions, that is, in a certain space, when the new effective temperature is 21^{o}C, it produces a thermal sensation like that experienced in quiet air at 21^{o}C, 50% humidity, and uniform radiation conditions. From here, we build a spreadsheet according to Thom's formula with the air temperature at 50% humidity (equivalent to dry temperature) and determine the classification of heat sensation for people in specific tropical regions like Vietnam (Table 4). In terms of geographical distribution, Vietnam stretches from latitude 8^{o}27' to 23^{o}23' North, with high mountainous terrain in the north of the country, so the temperature background of Vietnam is quite diverse. In the Northern regions, the temperature is more extreme with 4 distinct seasons. Meanwhile, HCMC has a more moderate temperature background (VGP, 2021). According to statistics in recent years from the Southern Hydrometeorological Station, in HCMC, the highest and lowest air temperatures were 38^{o}C and 16^{o}C (equivalent level from 2 to 6). Therefore, this scale will not consider the thresholds of DI less than 15^{o}C and greater than 33^{o}C. Finally, we have developed an appropriate DI index scale for HCMC, including 5 levels as shown in Table 5.

Table 4. Comfort thresholding based on an effective temperature scale applied to Vietnam.

Level	Ta (^{o}C)	Thermal feeling	Comfort feeling	Rh (%)	DI (^{o}C) calculated from Ta and Rh
1	<15	Very cold	Very cold	50	<15
2	15 - 20	Cold	Cold	50	15-19
3	>20 - 25	Cool	Comfort	50	19-22
4	>25 - 30	Warm	Less Comfort	50	22-26
5	>30 - 35	Hot	Discomfort	50	26-29
6	>35 - 40	Very hot	Very Discomfort	50	29-33
7	>40	Extreme hot	Emergency dangerous situation	50	>33

(In this table, the first 5 columns on the left were referenced from Nguyen (2008), the last column on the right - the DI value - was the authors)

Table 5. UTC levels by DI classification suitable for HCMC climatic conditions.

TT	UTC level	DI (^{o}C)
1	Cold	< 19
2	Comfort	$19 \leq DI < 22$
3	Less Comfort	$22 \leq DI < 26$
4	Discomfort	$26 \leq DI < 29$
5	Very Discomfort	≥ 29

Component parameters involved in calculating DI from remote sensing data

In the formula for calculating DI, it is necessary to determine the air temperature Ta and relative air humidity Rh. These two parameters are intrinsically related to the composition of the Earth's surface, which involves the surface temperature (Ts) and the land cover components. Many studies have shown there is a strong relationship between Ts and Ta, although the two temperatures have different physical meanings and responses to atmospheric conditions. Most studies found linear correlations between Ts and Ta (Kawashima et al., 2000; Mutiibwa et al., 2015; Good et al., 2017; Hadria et al.,

2018; Sun, 2020). In addition, the NDVI represented for the land cover had significant linear positive linkages with relative humidity (Wang et al., 2004; Huang, 2006).

This study used Landsat images to estimate Ts and NDVI. From here, Ta and Rh were calculated according to the empirical equations built by statistical methods. Firstly, the pre-processing procedure of the Landsat image was carried out with radiometrically and geometrically correction. The image was radiometrically corrected by applying the radiance-based procedure recommended by USGS (Montanaro, 2014; Barsi et al., 2014; Micijevic et al., 2016), which involves converting the raw digital number (DN) values to spectral radiance and then to at-sensor reflectance for the visible and infrared bands. Next, the image was georeferenced to the Universal Transverse Mercator (UTM) projection system using projection parameters suitable for Vietnam VN-2000. Calculation of each physical parameter used to estimate DI is described below.

Land surface temperature

Thermal infrared spectroscopy is fundamentally different from visible to near-infrared and shortwave infrared spectroscopy because most thermal infrared systems involve detecting emitted radiation instead of reflected radiation (Bedell et al., 2017). The theory to express the thermal emission is based on the black body concept. A black body, however, emits radiation as well; its magnitude depends on its temperature and is expressed by Planck's Law. This temperature is named brightness temperature, which is a directional temperature obtained by equating the measured radiance (B_λ) with the integral over the wavelength of Planck's black body function multiplied by the sensor response. Planck's blackbody equation (Markham and Barkewr, 1986) was used to convert brightness temperatures (T_B) from spectral radiances as Equation 3.

$$T_B = \left(\frac{hc}{k\lambda}\right)\left(\frac{1}{\ln\left(\left(2hc^2\lambda^{-5}\right)/B_\lambda + 1\right)}\right) \quad \text{(Eq.3)}$$

where, h – Planck constant (6,62 $\times 10^{-34}$ J-sec); c – speed of light (2,998 $\times 10^{8}$ m sec^{-1}); λ - emitted radiation wavelength (μm); k – Boltzmann constant (1,38x10^{-23} JK^{-1}); B_λ - radiation on satellite in wavelength λ ($Wm^{-2}\mu m^{-1}$).

The surface temperature Ts, as defined from Stefan-Boltzmann's law after transformation, is determined by Equation 4 (Gupta, 1991).

$$T_S = \frac{1}{\varepsilon^{1/4}} T_B \quad \text{(Eq.4)}$$

where ε is land surface emissivity with values from 0 to 1 and calculated by Equation 5 (Valor and Caselles, 1996).

$$\varepsilon = \varepsilon_v P_v + \varepsilon_s (1 - P_v) \quad \text{(Eq.5)}$$

where ε_v, ε_s represent the emissivity of vegetation and soil, respectively; P_v is the fraction of the vegetation presence in pixel, calculated by Normalized Differential Vegetation Index (NDVI) correlating with threshold values of $NDVI_s$ of bare land or $NDVI_v$ of vegetated land. The ratio formula determines P_v in Equation 6 (Carlson and

Ripley, 1997).

$$P_V = \left(\frac{NDVI - NDVI_S}{NDVI_V - NDVI_S}\right)^2 \quad \text{(Eq.6)}$$

The NDVI is determined based on the different reflectance of vegetation shown between the red reflectance (RED) band in the visible spectrum and the near-infrared spectral band (NIR) (Townshend and Justice, 1986).

$$NDVI = \frac{NIR - RED}{NIR + RED} \quad \text{(Eq.7)}$$

Building functions to simulate air parameters

This study has investigated the correlation between air temperature and humidity observed from the meteorological stations (Fig. 1 and Table 2) with values calculated from satellite images to build regression functions to simulate their spatial distribution. Popular criteria were used to assess the performance of the regression model: the correlation coefficient R, determination coefficient R^2, Sig-F, and t-Stat that was calculated from linear regression analysis. The following simple linear regression model was constructed to estimate the Ta and Rh:

$$Ta = a*Ts + b \quad \text{(Eq.8)}$$

$$Rh = c*NDVI + d \quad \text{(Eq.9)}$$

where a, b, c, and d are coefficients of regression, which are estimated using ordinary least squares regression.

The air temperature is directly influenced by the radiant heat of the underlying surface. Therefore, we built the relationship between surface temperature retrieved from the satellite image and air temperature collected from meteorological stations. The independent variable was the surface temperature Ts, and the dependent variable was the air temperature Ta. Checking the suitability of the regression model was carried out through the following criteria: Sig-F = 0.002 < 0.05 is significant; t-Stat = 5.20 > 2 is consistent with the 5% significance level. There was a strong correlation between surface temperature and air temperature when the correlation coefficient R = 0.905 and the coefficient of determination R^2 = 0.82. It proved that Ta and Ts had a close relationship, so the regression model was suitable. The linear regression equation had the following formula:

$$Ta = 0{,}7219*Ts + 1{,}2964 \quad \text{(Eq.10)}$$

Air humidity represents the humid state of the environment and is also influenced by the humidity of the underlying surface cover layer. Therefore, there is a close relationship between humidity and vegetation cover (Wang et al., 2004; Huang et al., 2016). In places with many trees, the air humidity is usually high, while it is usually low in bare land or sparse green trees. This study established the relationship of air humidity with the NDVI vegetation index image. The NDVI image was the independent variable,

and the air humidity was the dependent variable. Checking the suitability of the regression model is carried out from the following criteria: Sig-F = 0.0005 < 0.05 is significant; t-Stat = 3.81 > 2 is consistent with the 5% significance level. The correlation coefficient between air humidity and the NDVI index was strong with R = 0.904 and R^2 = 0.82. It proved that Rh and NDVI had a good relationship, so the regression model was suitable. The linear regression equation for estimation of humidity was defined as the following:

$$Rh = 25{,}758 * NDVI + 62{,}185 \quad \text{(Eq.11)}$$

Validation of the Landsat-estimated results

Three parameters, including Bias, Root-Mean-Square Error (RMSE), and Percentage of Error (PE), were calculated to validate the Landsat-estimated results compared with observed ground data obtained from standard meteorological stations. X_i and Y_i were estimated values and ground data values, respectively. N was the number of samples. These parameters were defined as the following:

$$\text{Bias} = \frac{1}{n}\sum_{i=1}^{n}\left(X_i - Y_i\right) \quad \text{(Eq.12)}$$

$$\text{PE} = \frac{1}{n}\sum_{i=1}^{n}\left|\frac{X_i - Y_i}{X_i}\right| \times 100 \quad \text{(Eq.13)}$$

$$\text{RMSE} = \sqrt{\frac{1}{n}\sum_{i=1}^{n}\left(X_i - Y_i\right)^2} \quad \text{(Eq.14)}$$

Land cover classification

Land cover classification can be carried out by a variety of methods. The NDVI (Normalized Differential Vegetation Index) is a commonly used index to measure greening by vegetation and is also an expression of land cover types determined from threshold levels in the range -1 to +1 (Meera Gandhi et al., 2015; Jeevalakshmi et al., 2016; Zhao et al., 2017). In this study, the land cover was classified into 4 types: built-up land, bare land, vegetation, and water bodies.

According to the survey on processed image data of this study, suitable threshold levels of NDVI values for land cover types were determined as follows: (1) NDVI < -0.26 corresponds to the water bodies type, which is the area of rivers, lakes, and ponds; (2) -0.26 ≤ NDVI < 0.1 corresponds to built-up land type including urban areas, roads, concretized vacant land areas, industrial parks, etc. with closed surfaces, does not allow water to penetrate below and often occurs surface overflow; (3) 0.1 ≤ NDVI < 0.2 corresponds to the type of bare land, which is the area of abandoned land or undeveloped land; (4) NDVI > 0.2 corresponds to vegetation cover type, representing land with crops and trees in residential areas.

Accuracy assessment was used to measure the compatibility between classification results with the real land cover conditions in the field. The minimum land cover classification accuracy requirement is about 85% (Lillesand and Kiefer, 1990). To evaluate the accuracy of land surface cover classification, we used a set of test samples selected through a combination of visual surveys on original satellite images, Google Earth images, and field information. Each land cover type was accurately sampled from the color composite image in points distributed throughout the study area. The number of points was about 200. These samples were then used to calculate the confusion matrix for the classifier to define the error statistics (Congalton, 1991; Lusch and Hudson, 1999). The accuracy assessment results showed 90% overall accuracy and 0,89 for Kappa, which means the land cover classification was valid for further analysis.

Results and discussion

The land cover spatial distribution

The Landsat image of the NHCMC was classified into 4 land cover classes: built-up land, bare land, vegetation, and water bodies. Each land cover type occupies landmasses, as shown in Table 6 and Fig. 2 below. The overall analysis showed that the space of vegetation cover was mainly distributed in 4 suburban districts and riverside areas. Built-up land space has been concentrated in the middle of the existing urban districts and most of the newly developed urban districts. The water bodies were scattered around rivers and lakes, interspersed within the city and along the eastern boundary of the Saigon River. Statistical results of each layer cover percentage showed that the vegetation cover accounted for the highest percentage of about 52.74%, equivalent to about half of the entire study area. Next was the built-up land cover, which accounted for about 35.73%, equivalent to more than 1/3 of the entire area. The lowest was the water surface layer, which accounted for nearly 4% of the entire area. The uneven distribution of land cover types shows a high concentration of urban areas in the core of HCMC and gradually dispersed to the periphery of the city.

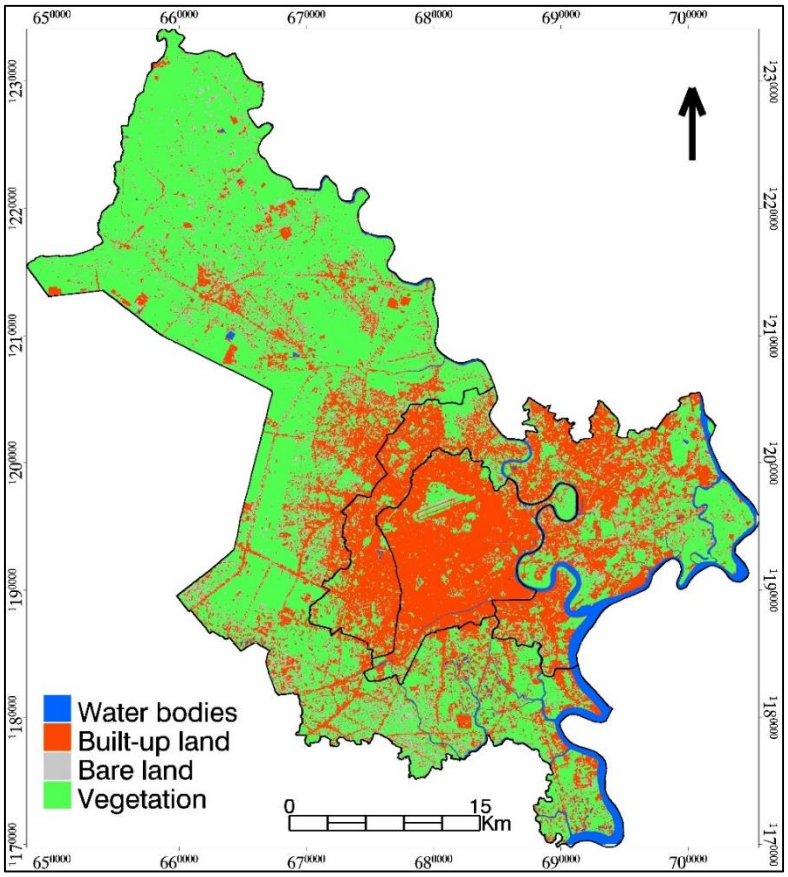

Fig. 2. Map of land cover distribution in the study area in the dry season of 2019

Table 6. Area percentage (%) of distribution of land cover types

Land cover type	Z1	Z2	Z3	Z1+Z2	Total
Built-up land	81.14	53.24	21.67	61.26	35.73
Bareland	4.18	7.63	8.25	6.64	7.68
Vegetation	12.36	31.50	67.45	26.00	52.74
Water bodies	2.32	7.63	2.63	6.10	3.85
Total	100	100	100	100	100

Considering the division of administrative units, the comparison between zones shows that, in Z3, the suburbs of NHCMC, which is considered as the green belt of the city, the vegetation cover has reached 67.45% of the whole area, that was 3 times more when compared to the built-up land cover, accounting for only 21.67% respectively. In Z2, which is the area of 6 newly developed urban districts, the built-up land factor has accounted for more than half of the area with 53.24%; vegetation and water covers accounted for about 31.5% and 7.63% respectively. In Z1 - 13 existing urban districts, considered as the core urban area of HCMC, where the built-up land class was a predominance, accounting for 81.14%, equivalent to 4/5 of the area of the whole region. Meanwhile, the vegetation cover has reached about 12.36%, and the water surface cover has accounted for more than 2%. At the end of 2018 was 4,042,112 people in the city (PSO 2018). If calculating the area of green trees per capita, it reached only

4.34m^2/person, lower than the standard requirement of TCVN 9257:2012, 12-15 m^2/person (VNS-TCVN, 2012).

Meanwhile, the UN's target is set at a minimum of 10 m^2/person. This figure was also very low compared to some countries such as Singapore 30.3 m^2/person, Seoul 41 m^2/person, Berlin 50 m^2/person, etc. (Phan Hau, 2021). Z1 has shown the characteristics of urban areas with a high density of the population and a dense impervious surface, resulting in the temperature in the core urban area consistently higher than in the surrounding suburbs, which led to the formation of urban heat islands (Van, 2010). It is a form of local climate change caused by human impacts. It occurs when the temperature within the city is greater than the temperature of the surrounding suburban areas. Many factors contribute to the formation of urban heat islands. However, the first factor is the loss of vegetation cover and the replacement of the land surface with impermeable materials that cause less water to enter the atmosphere than from the natural surface (Lo et al. 1997). This does not guarantee a good quality of life for urban residents. If comparing urban areas (including Z1 and Z2) and suburban areas (Z3), the picture of the element "urban - vegetation cover" was almost opposite in value (61% - 26%) and 22% - 67%, respectively.

HCMC is a unique city, a major center of economy, culture, science, and technology. According to the orientation, by 2025, the city's population will be about 10 million people. The scale of urban land construction is about 90,000 - 100,000 ha, of which the existing urban (Z1) is 14,000 ha, the newly developed urban area (Z2) is about 35,000 ha, and the suburban area (Z3) is about 40,000 - 50,000 ha (Prime Minister, 2010). Since the central urban area has been completely urbanized, the city continues to expand to the suburbs, building satellite towns to reduce population pressure on the central area. With such a strong urban development, the problem of urban environment will become worse and worse. The process of urbanization and the pressure of urban space development to serve this urbanization process have made green areas, impervious surfaces, and natural open water sources have been gradually replaced by construction works, houses, roads, residential areas, and industrial parks. The increase in the impervious surface area, the decrease in the green area, and the narrowing of the open water surface is the main cause of the increase in surface temperature. It leads to the difference in thermal comfort levels between areas. The decrease in thermal comfort has caused unpleasant sensations to the body, affecting public health.

Spatial patterns of Urban Thermal Comfort over NHCMC

Thom's discomfort index was estimated from air temperature and humidity, constructed based on surface properties according to land surface temperature and vegetation index. The result is a map of DI distribution over a study area with a detailed level of Landsat satellite image resolution of 30m. Then DI values were classified according to the specified range of values from Table 5. This map shows the spatial patterns of UTC in the study area.

Landsat-estimated values were compared with observed ground values calculated from data obtained from 3 national meteorological stations to validate the conducted method. These stations are within the NHCMC. Tan Son Hoa and Tan Son Nhat are located in a densely populated area, while Nha Be station is in the suburbs. Statistical analysis was conducted to investigate the method's accuracy. We performed comparisons for the 3 parameters Ta, Rh, and DI in 3 categories: Bias, PE, and RMSE

(Table 7). The comparison results achieved from the image-estimated and meteo-station-calculated equations can indicate reliable accuracy.

Table 7. Validation of Landsat-estimated DI with calculated DI from measured values at meteorological stations

Meteorological station	Landsat-estimated	meteo-station-calculated	Bias	PE
Ta (°C)				
Tan Son Hoa	28.0	29.5	-1.5	5.36
Tan Son Nhat	28.8	30.0	-1.2	4.17
Nha Be	28.3	29.8	-1.5	5.30
Average			-1.4	4.94
RMSE			1.40	
Rh (%)				
Tan Son Hoa	59.0	54.0	5.0	8.47
Tan Son Nhat	57.2	58.6	-1.4	2.45
Nha Be	55.0	53.0	2.0	3.64
Average			1.87	4.85
RMSE			3.21	
DI (°C)				
Tan Son Hoa	25.0	25.7	-0.7	2.8
Tan Son Nhat	25.4	26.5	-1.1	4.33
Nha Be	24.9	25.8	-0.9	3.61
Average			-0.9	3.58
RMSE			0.91	

Table 8 shows the distribution percentage across the whole region in the total column and by zone for NHCMC in the dry season of 2019. As shown in Fig. 3, on NHCMC, the most common was the pattern of Less Comfort-type UTC, which occupied about 3/4 of the entire area (equivalent to about 75.95%). Next, Comfort-type UTC has taken up about 17.89%, or nearly 1/5 of the entire area. UTC of Discomfort types accounted for approximately 2.5%. UTC of Very Discomfort type existed with a very small proportion of only about 0.04%, equivalent to 33 hectares.

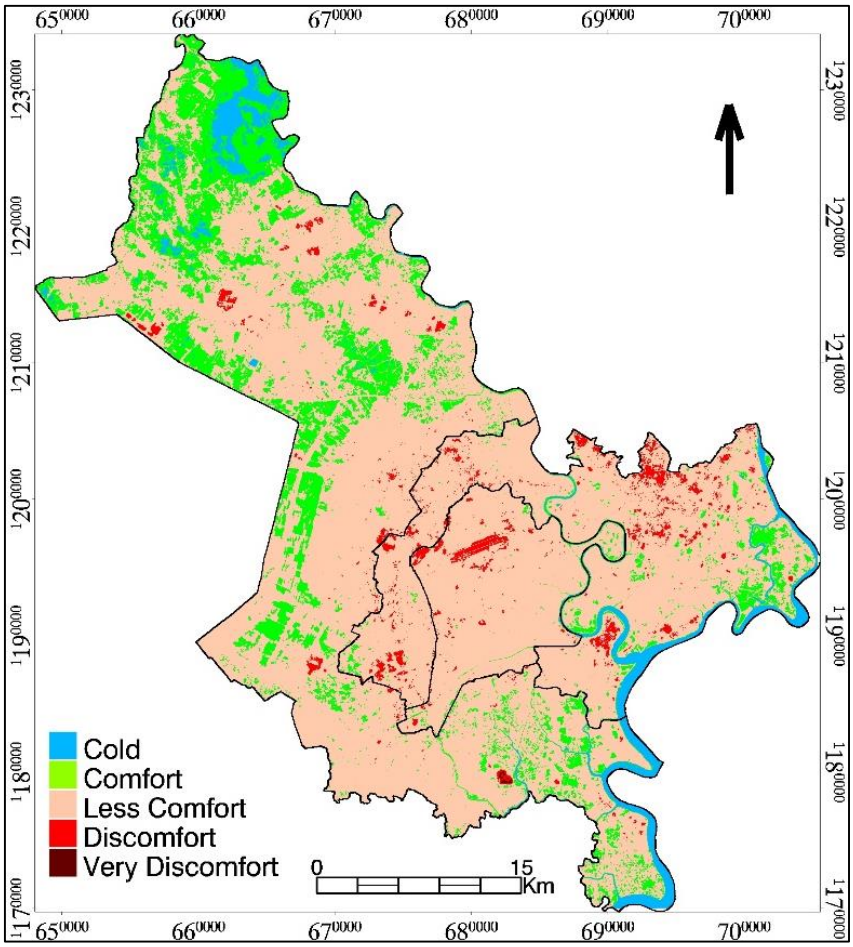

Fig. 3. Map of spatial patterns of UTC of the study area in the dry season of 2019

Table 8. Area percentage (%) of distribution of thermal comfort levels by administrative zone

UTC level	Z1	Z2	Z3	Z1+Z2	Total
Cold	0.98	6.32	3.06	4.78	3.67
Comfort	2.02	6.71	24.80	5.36	17.89
Less Comfort	92.42	81.59	71.13	84.71	75.95
Discomfort	4.58	5.38	0.97	5.15	2.45
Very Discomfort	0.00	0.00	0.04	0.00	0.04
Total	100	100	100	100	100

When analysing administrative zones, the spatial distribution of Comfort-type UTC in Z1 was insignificant, accounting for only about 2.02% of that total area. Meanwhile, the Discomfort type took up twice the space of the Comfort type. Most UTC in this region was Less Comfort type, taking up most area space. The suburban Z3 had the opposite spatial distribution of UTC to Z1, while the Comfort-type UTC had a larger expansion of 24.80%, accounting for a quarter of the entire Z3 area. Meanwhile, Discomfort-type UTC was scattered about less than 1% of the area. Especially at Z3, tiny areas occupied only 0.04% of Very Discomfort-type UTC. The most obvious was the site of Da Phuoc Integrated Waste Management Facility with an open-air landfill of the whole city comes here, and some neighboring industrial zones. Z2 are newly developed urban areas with the same image as Z1, where most areas were Less

Comfort-type UTC. But we found the portion of Discomfort UTC smaller than of Comfort ones.

Variation of Urban Thermal Comfort across Different Landcover Types

To better understand the urban thermal environment for quality-of-life concerns when people feel comfortable or uncomfortable, we performed an assessment of the difference of UTC by land cover patterns as presented in Table 9.

Table 9. Area percentage (%) of variation of UTC across different landcover types.

UTC level	Built-up land	Bare land	Vegetation	Water	Total
Cold	0.94	0.33	17.81	80.92	100
Comfort	2.98	1.27	90.97	4.78	100
Less Comfort	43.79	9.38	46.77	0.06	100
Discomfort	75.85	12.77	11.38	0.00	100
Very Discomfort	89.84	5.61	4.55	0.00	100

At the Cold UTC level, the threshold when the human body feels uncomfortable from the cold due to low temperature, it was dominated by the water bodies cover type, which was equivalent to 4/5 the area of all landcover types this comfort level. At the Comfort Level, the green factor was evident, precisely the vegetation cover type occupied about 9/10 of the area of all cover types in this level. At the Less Comfort level, for NHCMC, it appeared on built-up land with a ratio of nearly half the area of all land covers. We mainly found built-up land at the remaining two levels, Discomfort and Very Discomfort UTC, taking up about 3/4 and 9/10 of all land covers, respectively. Field identification and detecting details on satellite images showed that the Cold UTC level with the largest distribution area was mainly found in rivers with wide-open surfaces in the cover type of water bodies. These places often have relatively low temperatures and are not suitable for living. However, on this land cover type, 4.78% of the area was distributed at the Comfort level. These were small water areas such as ponds and lakes partially affected by the surrounding heat, so they became places with a Comfort level. The dense green area with high canopy height provided a comfortable living environment, comfortable space, and no heat stress in the vegetation cover type. Therefore, most of the distribution area was of the Comfort level. However, we still detected Discomfort on this vegetation cover type, even Very Discomfort types with a total area of about 15%. These were places with sparse greenery mixed with bare land and dense urban zones, so they were affected by the heat from these two objects.

Fig. 4 shows the locations of areas with UTC at Very Discomfort and Discomfort levels on the bivariate choropleth map of UTC and land cover (LC). Bivariate Choropleth map is a correlation map - a cartographic technique that aggregates individual incidences according to a set of data collection units and then colors each unit by its aggregate value (Slocum et al., 2008). Bivariate choropleth maps combine two datasets (usually numerical data) into a single map allowing us to show relatively how much X (variable 1) and Y (variable 2) exist in each enumeration unit (Aix Map, 2020). From this map, the highest levels of UTC correlated with the built-up land.

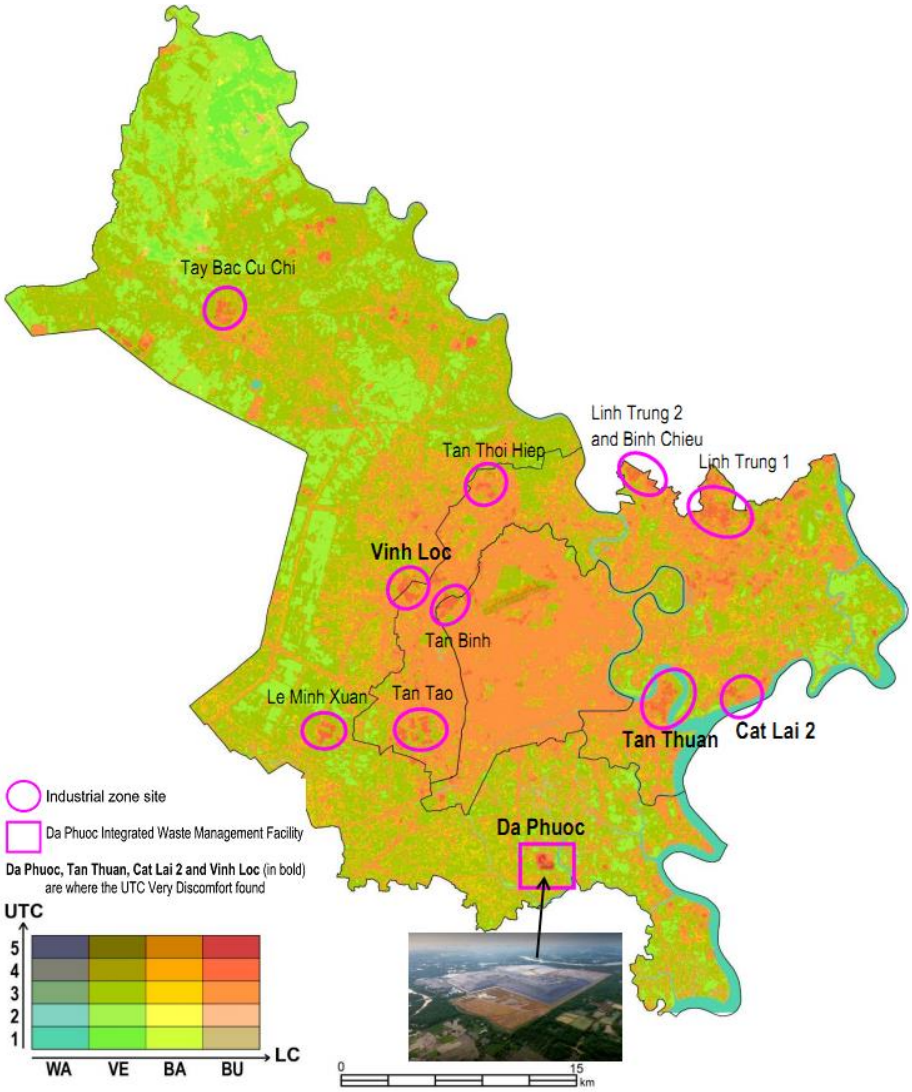

Fig. 4. Location of industrial zones with UTC Very Discomfort and Discomfort

(This bivariate choropleth map integrated by UTC and LC components, where X-axis is LC with WA - water, VE - vegetation, BA – bare land, BU - built-up land; Y-axis are UTC levels with 1 - Cold, 2 - Comfort, 3 - Less Comfort, 4 - Discomfort, 5 - Very Discomfort)

There were 4 positions on the Very Discomfort level to be found. At the top was the Da Phuoc Integrated Waste Management Facility with the landfill, which has received all of HCMC's waste and treated it with landfill technology. Decaying garbage under the direct sunlight of the Sun resulted in the temperature here always being much higher than in the surrounding areas. The other 3 locations were industrial zones, including Cat Lai 2, Tan Thuan, and Vinh Loc. The remaining positions of the other industrial zones had UTC levels of Discomfort. These are places where production activities serve the socio-economic development of HCMC. The heat-absorbing and retaining properties of the building materials of the factories, plus the amount of heat emitted from the production process, have caused these places always to have a higher temperature than the surrounding locations with the other land cover type. In the past, these locations were in the suburbs where crops were grown in agricultural land, and the land surface was regularly covered with green vegetation. Many years ago, the city government

moved production facilities out of urban residential areas into these suburbs. Growing urbanization has expanded residential housing areas to encroach on this agricultural land, so industrial zones are mixed in urban areas today. The situation of building expansion, encroaching on the surrounding countryside, is growing massively. Significantly, the leveling of ponds and lakes takes away the inherent natural water surface of the city, causing the urban landscape to change constantly. That leads to an increasingly harsh urban thermal environment.

The above spatial patterns clearly show that, in NHCMC, the distribution of construction and green land was not reasonable, making urban outdoor always a place where people feel uncomfortable. Urban areas in NHCMC was mostly just construction surfaces with impervious covers such as concrete, asphalt, tile roofs, making these surfaces easily heated by solar radiation during the day. They have good heat-absorbing properties and store this heat beneath this impermeable surface layer. At night, they radiate heat back into the air, making the air environment in urban areas always warm. When people live in such an environment surrounded by constant heat, they will need to be cooled to feel comfortable, which leads to the constant use of cooling fans and air conditions. In turn, these devices will release heat into the surrounding air, contributing to urban heating. NHCMC is a developing city, so there are still many shortcomings in terms of emissions into the air, causing air quality to go down. At this time, the high-temperature environment inside the urban area will cause the aerosol emission to be increased more. They will linger in the upper air layer, easily causing direct harm to urban residents when inhaled. For residents of the poor class who can not afford adequate cooling equipment, the suffocating heat brings, easily making their nerves unstable; thereby leading to criminal acts or self-harm. That reduces the quality of life in the city.

Conclusion

The present study built a spatial distribution map of UTC patterns in NHCMC from Landsat satellite imagery in the dry season of 2019, with the Less Comfort pattern occupying most of the study area. Besides, the land cover types have also been classified, showing a high concentration distribution of built-up land in the 19 central urban districts. This type of built-up land was found to have the highest weight on the Discomfort and Very Discomfort type UTC zones. In particular, all existing industrial zones are locations with these two dangerous levels of thermal discomfort. To determine spatial patterns of UTC, we built spatial distribution images of air temperature and humidity from the parameters of Landsat images, including LST and NDVI, to integrate them into the DI calculation formula. At the same time, we have also built a 5-level classification scale of DI to distinguish UTC levels for HCMC, one of the cities with tropical climate characteristics. From here, it is shown that the different thermal comfort levels in different areas are due to the density of urbanization, industrial zones, open water areas, greenery, and impervious surface. Suburban areas often had better thermal comfort due to sparse built-up land, lots of trees, and rivers.

These results support the need for an increased effort to create useful remotely sensed data sources applied to environmental, public, and industrial health practices. Landsat data are the most consistent and widely available source of relatively high-resolution thermal information from satellites but can be limited due to the number of clear images available on certain days and times. However, the continued acquisition of

these data with comparable resolution has the potential to provide important spatial information about the outdoor comfort of a city or region.

This study is the answer to the urgent measures needed for the urban government of HCMC to rebuild the master plan for the urban landscape. Socio-economic development cannot but be associated with quality of life, in which thermal comfort is an important indicator that needs to be considered to evaluate. This study shows that the built-up land area is mainly the inner city, where the population is concentrated, subject to thermal discomfort due to the hot thermal environment, whereas suburban areas achieve the most Comfort level, thanks to a higher density of trees. In the master development planning strategy, city managers need to pay more attention to the reasonable allocation of construction density and trees to minimize heat intensification, avoid reducing the quality of life and ensure safety and comfort for city residents. In addition, there must be a policy to issue documents on rational planning of urbanized areas, limiting migration from rural to urban areas, managing planting and expansion of green areas, and conserving surface water resources. It is necessary to encourage the "green roof" model to reduce the temperature of the residence and green the city.

Acknowledgement

Disclosure statement

Authors' contributions

References

Adegoke, O.O., Dombo, T.P., 2019. Geospatial Modeling of Human Thermal Comfort in Akure Metropolis Using Thom's Discomfort Index. *International Journal of Environment and Bioenergy* 14(1): 40-55.

Ahmed, A.B., Ifeoluwa, A.B., Zachariah, D.A., 2010. Comparisons of urban and rural heat stress conditions in a hot_humid tropical city. *Global Health Action* 3: 5614 - DOI: 10.3402/gha.v3i0.5614

Axis Map, 2019. Bivariate Choropleth. Online: https://www.axismaps.com/guide/bivariate-choropleth (accessed May 1 2019).

Barsi, J.A., Schott, J.R., Hook, S.J., Raqueno, N.G., Markham, B.L., Radocinski, RG., 2014. Landsat-8 Thermal Infrared Sensor (TIRS) Vicarious Radiometric Calibration. *Remote Sens*. 6: 11607-11626.

Bedell, R.L., Rivard B., Browning D., Coolbaugh, M., 2017. Thermal Infrared Sensing for Exploration and Mining – An Update on Relevant Systems for Remote Acquisition to Drill Core Scanning. *In Proceedings of Exploration 17: Sixth Decennial International Conference on Mineral Exploration*, edited by V. Tschirhart and M.D. Thomas, 2017, p. 881–897

Bradshaw, V., 2006. *The Building Environment: Active and Passive Control Systems*. 3rd edition. John Wiley & Sons, Inc. Hoboken, New Jersey

Campbell, J.B., 1987. *Introduction to Remote Sensing*. New York: The Guilford Press.

Carlson, T., Ripley D., 1997. On the relation between NDVI, fractional vegetation cover and leaf area index. *Remote sensing of Environment* 62: 241-252.

Congalton, R.G., 1991. A review of assessing the accuracy of classifications of remotely sensed data. *Remote Sens Environ*. 37(1): 35–46.

Fanger, P.O., 1970. *Thermal Comfort: Analysis and applications in environmental engineering*. New York: McGraw-Hill.

Gupta, R., 1991. *Remote Sensing Geology*. Germany: Springer-Verlag Berlin Heidelberg.

Hamidreza, H., Farideh, G., Aliakbar, S., Abbas, R.F., Abbasali, G., 2014. Evaluation of Thermal Discomfort in Outdoor Environments: A Cross Sectional Study throughout IRAN. *Advances in Environmental Biology* 8(13): 1008-1015

Höppe, P., 1999. The physiological equivalent temperature – a universal index for the biometeorological assessment of the thermal environment. *Int J Biometeorol*. 43: 71–75.

Huang, F., Wen, D.H., Wang, P., 2016. Vegetation changes and the relationship with climate variability in the upper and middle reaches of the Nenjiang river basin, China. *The International Archives of the Photogrammetry, Remote Sensing and Spatial Information Sciences*, Volume XLI-B8, XXIII ISPRS Congress, 12–19 July 2016, Prague, Czech Republic.

Ifeoluwa, A.B., Ahmed, A.B., 2013. Urban heat island and bioclimatological conditions in a hot-humid tropical city: the example of Akure, Nigeria. *Journal of the Geographical Society of Berlin* 145(1-2): 3-15. DOI: 10.12854/erde-145-2.

Jeevalakshmi D., Reddy S.N., Manikiam B., 2016. Land cover classification based on NDVI using LANDSAT8 time series: A case study Tirupati region. In proceedings of 2016 *International Conference on Communication and Signal Processing (ICCSP*). p. 1332-1335.

José, A.S., Rosa, O.C., Guillem, S., Juan, C.J.M., Belén, F., Victoria, H., Cristian, M., Yves, J., Juan, C., Mireia, R., Antonio, G., Eduardo, D.M., Remo, B., Marc, P., 2013. Evaluation of the surface urban heat island effect in the city of Madrid by thermal remote sensing. *International Journal of Remote Sensing* 34(9-10): 3177–3192, http://dx.doi.org/10.1080/01431161.2012.716548

Kawashima, S., Ishida, T., Minomura, M., Miwa, T., 2000. Relations between Surface Temperature and Air Temperature on a Local Scale during Winter Nights. *Journal of Applied Meteorology* 39(9): 1570-1579.

Keeler, J.M., Kristovich, D.A.R., 2012. Observations of urban heat island influence on lake-breeze frontal movement. *Journal of Applied Meteorology and Climatology* 51(4): 702-710.

Kyle, W., 1999. The human bioclimate of Hong Kong. In: Brazdil, R. and Kolar, M., Eds., Contemporary Climatology. *Proceedings of COC/IGU Meeting*, 15-20 August 1994, Masaryk University, Brno. p. 345–350.

Lee, A.C., Jordan, H.C., Horsley, J., 2015. Value of urban green spaces in promoting healthy living and wellbeing: prospects for planning. *Risk Manag Healthc Policy* 8: 131-137.

Li, D., Bou-Zeid, E., 2013. Synergistic interactions between urban heat islands and heat waves: The impact in cities is larger than the sum of its parts. *Journal of Applied Meteorology and Climatology* 52(9): 2051-2064.

Lillesand, T.M., Kiefer, R.W., 1990. *Remote Sensing and image interpretation*. 3rd ed. New York: John Wiley&Son.

Lo, C.P., Quattrochi, D.A., Luvall, J.C., 1997. Application of high resolution thermal infrared remote sensing and GIS to assess the urban heat island effect. *International Journal of Remote Sensing* 18: 287−304.

Lusch, D.P., Hudson, W.D., 1999. *Introduction of Environmental Remote Sensing*. Michigan State University. (accessed 2021 June 10).

Markham, B.H.jL., Barkewr, J.L., 1986. Landsat MSS and TM Post Calibration Dynamic Ranges, Exoatmospheric Reflectance and at-satellite Temperatures. *EOSAT Landsat Technical Notes* 1, 3–8

Meera, G.G., Parthiban, S., Nagaraj, T., Christy, A., 2015. NDVI - Vegetation Change Detection Using Remote Sensing and GIS – A Case Study of Vellore District. *Procedia Computer Science* 57: 1199-1210.

Mayer, H., Holst, J., Dostal, P., Imbery, F., Schindler, D., 2008. Human thermal comfort in summer within an urban street canyon in Central Europe. *Meteorologische Zeitschrift* 17: 241-250.

Micijevic, E., Haque, M.O., Mishra, N., 2016. Radiometric calibration updates to the Landsat collection. *Proc. SPIE 9972*, Earth Observing Systems XXI, 99720D, September 19, 2016. San Diego, California, United States.

Montanaro, M., Lunsford, A., Tesfaye, Z., Wenny, B., Reuter, D., 2014. Radiometric Calibration Methodology of the Landsat 8 Thermal Infrared Sensor. *Remote Sens* 6: 8803-8821.

Mutiibwa, D., Strachan, S., Albright, T., 2015. Land Surface Temperature and Surface Air Temperature in Complex Terrain. *IEEE Journal of Selected Topics in Applied Earth Observations and Remote Sensing* 8: 4762-4774.

Nastos, P.T., Matzarakis, A., 2006. Weather impacts on respiratory infections in Athens, Greece. *International Journal of Biometeorology* 50: 358–369

Nasution, A.D., Zahrah, W., 2018. Quality of Life: Public open space effects. *Asian Journal of Environment-Behaviour Studies* 3(10): 124-132.

National Assembly, 2015. Law on occupational safety and hygiene. *Official Gazette* No. 871 + 872/July 29, 2015

Nguyen, P.D., 2008. *Bioclimatic architecture - Bioclimatic design in Vietnamese architecture*. Hanoi: Construction Publishing House.

Pecelj, M., 2013. Bioclimatic indices based on the menex model example on Banja Luka. *Journal of the Geographical Institute "Jovan Cvijić"* 63(1): 1-10.

Phan Hau, 2021. Urban trees in Vietnam are only 1/5 of the world's minimum standards. Online: https://thanhnien.vn/tai-chinh-kinh-doanh/kinh-te-xanh/cay-xanh-do-thi-o-viet-nam-chi-bang-15-tieu-chuan-toi-thieu-the-gioi-1335346.html (accessed June 10 2021).

Pradhan, B., Shrestha, S., Shrestha, R., Pradhanang, S., Kayastha, B., Pradhan, P., 2013. Assessing climate change and heat stress responses in the Tarai region of Nepal. *Ind Health* 51(1): 101-112.

Prime Minister, 2010. Decision No. 24/QD-TTg dated January 6, 2010, on Approval to adjust the general construction planning of Ho Chi Minh City up to 2025.

[PSO] Ho Chi Minh City Statistical Office, 2018. Statistical Yearbook 2018. Online: http://www.pso.hochiminhcity.gov.vn/c/document_library/get_file?uuid=ce0ffd52-d8c5-4794-a808-0b39531f50ab&groupId=18 (accessed June 10 2021).

Slocum, T.A., McMaster, R.M., Kessler, F.C., Howard, H.H., Mc Master, R.B., 2008. *Thematic Cartography and Geographic Visualization*. (3rd ed.) Upper Saddle River, New Jersey: Prentice-Hall.

Stathopoulou, M.I., Cartalis, C., Keramitsoglou, I., Santamouris, M.K., 2005. Thermal remote sensing of Thom's Discomfort Index (DI): comparison with in situ measurements. *SPIE Proceedings* 5983: 59830K-1-9

Sun, T., Sun, R., Chen, L., 2020. The Trend Inconsistency between Land Surface Temperature and Near Surface Air Temperature in Assessing Urban Heat Island Effects. *Remote Sensing* 12: 1271.

Thom, E.C., 1959. *The discomfort index*. Weather wise. 12: 57–60.

Townshend, J.R.G., Justice, C.O., 1986. Analysis of the dynamics of African Vegetation using the normalised difference vegetation index. *International Journal of Remote Sensing* 7: 1435-1445.

Toy, S., Yilmaz, S., Yilmaz, H., 2007. Determination of bioclimatic comfort in three different land uses in the city of Erzurum, Turkey. *Building and Environment* 42(3): 1315-1318

Unger, J., 1999. Comparisons of urban and rural bioclimatological conditions in the case of a Central-European city. *Int.J. Biometeorology* 43(3): 139-144.

[USGS] U.S. Geological Survey, 2021. Landsat mission: Landsat 8. 2021. Online: https://www.usgs.gov/core-science-systems/nli/landsat/landsat-8?qt-science_support_page_related_con=0#qt-science_support_page_related_con (accessed June 10 2021).

[USGS] Earth observation website, 2019. Online. http://earthexplorer.usgs.gov (accessed May 1 2019)

Valor, E., Caselles, V., 1996. Mapping Land Surface Emissivity from NDVI: Evaluation of the surface urban heat island effect in the city of Madrid by thermal remote sensing. International Journal of Remote Sensing _Application to European, African and South American Areas. *Remote Sensing of Environment* 57: 167-184.

Van Tran Thi, 2010. Urban heat island under impact of urbanization in Hochiminh City from remote sensing data. *Science and Technology Development Journal* 13(3): 103-117.

[VGP] Vietnam Government portal, 2010. Online: http://www.chinhphu.vn/portal/page/portal/chinhphu/NuocCHXHCNVietNam/ThongTinTongHop/dialy) (accessed 2021 June 10).

[VNS-TCVN] Vietnam National Standards, 2012. Greenery planning for public utilities in urban areas. TCVN 9257:2012.

Wang, W.W., Zhu, L.Z., Wang, R.C., 2004. An analysis on spatial variation of human thermal comfort in Hangzhou. *Journal of Environmental Sciences* 16(2): 332-338.

Xu, H., Hu, X., Guan, H., He, G., 2017. Development of a fine-scale discomfort index map and its application in measuring living environments using remotely-sensed thermal infrared imagery, *Energy and Buildings* 150: 598-607.

Zhao, L., Zhang, P., Ma, X., Pan, Z., 2017. Land Cover Information Extraction Based on Daily NDVI Time Series and Multiclassifier Combination. *Mathematical Problems in Engineerin*g 57: 1199-1210